JACS
JOURNAL OF THE AMERICAN CHEMICAL SOCIETY

ARTICLE

pubs.acs.org/JACS

# All-Carbon Molecular Tunnel Junctions

Haijun Yan,[†] Adam Johan Bergren,[†] and Richard L. McCreery*[,†,‡]

[†]National Institute for Nanotechnology, National Research Council Canada, Edmonton, Alberta, Canada

[‡]Department of Chemistry, University of Alberta, Edmonton, Alberta T6G 2G2, Canada

Supporting Information

**ABSTRACT:** This Article explores the idea of using nonmetallic contacts for molecular electronics. Metal-free, all-carbon molecular electronic junctions were fabricated by orienting a layer of organic molecules between two carbon conductors with high yield (>90%) and good reproducibility (rsd of current density at 0.5 V <30%). These all-carbon devices exhibit current density−voltage ($J-V$) behavior similar to those with metallic Cu top contacts. However, the all-carbon devices display enhanced stability to bias extremes and greatly improved thermal stability. Completed carbon/nitroazobenzene(NAB)/carbon junctions can sustain temperatures up to 300 °C in vacuum for 30 min and can be scanned at ±1 V for at least $1.2 \times 10^9$ cycles in air at 100 °C without a significant change in $J-V$ characteristics. Furthermore, these all-carbon devices can withstand much higher voltages and current densities than can Cu-containing junctions, which fail upon oxidation and/or electromigration of the copper. The advantages of carbon contacts stem mainly from the strong covalent bonding in the disordered carbon materials, which resists electromigration or penetration into the molecular layer, and provides enhanced stability. These results highlight the significance of nonmetallic contacts for molecular electronics and the potential for integration of all-carbon molecular junctions with conventional microelectronics.

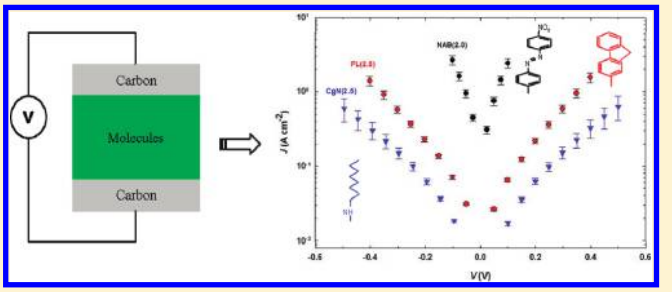


## 1. INTRODUCTION

Molecular electronics has been the center of extensive research efforts for the past decade.[1−8] This interest stems mainly from the prospect of fabricating functional electronic devices utilizing the diverse properties of organic molecules. Significant progress has been made in the field in terms of establishing various experimental paradigms and understanding charge transport through molecular electronic devices, both for single molecule experiments and in "ensemble" molecular junctions containing >1000 molecules oriented in parallel.[9−16] Although the formation of molecular layers on conducting substrates is generally well established and understood, it has been challenging to apply a "top contact" to complete the molecular junction while sustaining the integrity of the molecular layer. A variety of methods have been reported, including the use of liquid metals,[14,17,18] "soft" or "indirect" contact deposition,[19−23] break junctions,[9,12] and "direct" thermal or electron-beam deposition.[15,24,25] For direct deposition, the molecular layer is often found to be damaged or destroyed during top contact deposition, or the deposited metal penetrates into the molecular layer to form direct metal−substrate "short circuits".[26−31] Even if useful molecular electronic devices can be fabricated reliably, it is not yet clear how they can be integrated with the massively parallel fabrication techniques of conventional microelectronics, and whether they have sufficient temperature tolerance and operating lifetime. Our research group fabricates molecular junctions by electron-beam depositing a copper film onto a 1−5 nm thick molecular layer, which is covalently attached to a graphitic carbon substrate made from pyrolyzed photoresist film (PPF).[15,32−34] The molecular layer is usually bonded to the carbon substrate electrode by reduction of diazonium reagents, with the electrogenerated phenyl radicals forming a densely packed film with covalent C−C surface bonds. These carbon/molecule/Cu junctions can be made with very high yield (90−100%) and excellent reproducibility (typically rsd of current density at 0.5 V < 30%), are stable over a temperature range of 5−450 K, and can withstand at least $10^9$ current−voltage cycles to ±1 V in lab ambient.[33] We have thoroughly investigated charge transport characteristics and recently demonstrated microfabrication and integration of these Cu devices.[34] However, as we and others[35−37] have shown, Cu can undergo electro-oxidation under an applied bias to form conducting filaments in molecular junctions, and these metallic filaments can completely dominate device characteristics. While Au is electrochemically inert compared to Cu, Au atoms are mobile, and direct Au deposition usually results in penetration into molecular layers,[28,31,38] including those made with diazonium reduction. Different techniques have been employed to overcome the Au penetration problem: for example, by inserting a thin atomic-layer-deposited (ALD) film of $Al_2O_3$,[39] or by spin-coating a layer of conducting polymer (PEDOT:PSS) on top of the molecular layer to provide "buffer" layers between the molecules and the evaporated Au layer.[16] More recently, our group has reported

**Received:** July 15, 2011
**Published:** October 21, 2011

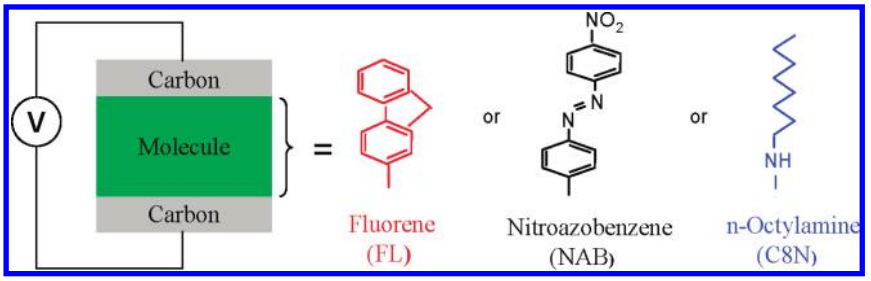


**Figure 1.** Schematic representation of a carbon/molecule/carbon molecular junction (left). The structures of molecules used in this work are shown on the right.

a novel technique of forming "soft" metallic contacts through surface-diffusion-mediated deposition (SDMD).[40] However, direct vapor deposition of contacts is still technologically advantageous in that it does not require extra fabrication steps and is readily compatible with existing semiconductor fabrication technology. Furthermore, "barrier metals" such as titanium nitride, tantalum nitride, and Ti/W alloy are preferred in the microelectronics industry over conventional metals due to their relative immunity to electromigration and diffusion. Therefore, an electrode material that is both electrochemically and thermally stable, does not easily undergo electromigration, and is compatible with existing CMOS technology is highly desirable for practical applications of molecular electronics.

Although the widespread interest in using fullerenes, graphene, and related carbon materials in carbon-based electronics is relatively recent,[41−45] $sp^2$-hybridized carbon electrodes have been used in electrochemistry for at least 100 years. Glassy carbon and graphite electrodes have a density of states distribution similar to that of a metal, but are covalent materials that are not subject to electromigration and are more stable than metals in an electrochemical environment. Furthermore, due to the chemical inertness of carbon electrodes, carbon-based electronic devices are particularly advantageous in biomolecular sensing applications or fast DNA sequencing where specific or nonspecific binding of biomolecules to metal electrodes is not desirable.

We chose pyrolyzed photoresist films (PPF) and electron-beam deposited carbon films (referred to as e-C hereafter) as substrates for fabricating carbon-based molecular junctions mainly due to the ability to irreversibly bond molecular layers to $sp^2$ carbon surfaces with a C−C bond.[34,46] Herein, we explore the use of disordered, $sp^2$ carbon as a nonmetallic top contact for molecular junctions, to result in a compositionally symmetric and metal-free carbon/molecule/carbon (i.e., "all-carbon") molecular junction. Carbon can be applied using electron-beam deposition, and carbon atoms or clusters should be much less mobile than metals once they deposit on a molecular layer. At least in principle, carbon deposition is compatible with conventional semiconductor processing techniques. We report below the properties of e-beam carbon as a top contact for molecular junctions, describe its advantages as compared to Cu and other metals, and discuss the electron transport characteristics of such all-carbon molecular electronic devices.

## 2. EXPERIMENTAL SECTION

Large-area molecular crossbar junctions (area ~0.0017 $cm^2$) were fabricated as previously described,[15,32,33,47] unless otherwise noted. Briefly, carbon bottom electrodes were prepared by pyrolyzing patterned photoresist stripes on thermally oxidized silicon wafers in a reducing atmosphere (5% $H_2$ and 95% $N_2$) at 1000 °C for 1 h. The pyrolyzed photoresist films (PPF) are partially graphitic and disordered carbon, resembling glassy carbon (GC) with a resistivity of 0.006 Ω cm.[48,49] The surface of PPF is flat, having a measured rms roughness similar to the substrate upon which it is made (in the current case, <0.5 nm by AFM[49]). Molecular layers of fluorene (FL), nitroazobenzene (NAB), or *n*-octylamine ($C_8N$) were deposited on PPF by the electrochemical reduction of the corresponding diazonium ions (FL and NAB) or oxidation of the primary amine ($C_8N$) in acetonitrile (with 0.1 M tetrabutylammonium tetrafluoroborate as supporting electrolyte). Note that both derivatization reactions are radical mediated, and multilayer formation is possible. However, molecular thicknesses can be controlled by varying the electrochemical derivatization conditions and are always verified by an AFM "scratching" technique, as previously reported.[50] Junction fabrication was completed by electron-beam deposition of top contacts through shadow masks oriented perpendicular to the PPF stripes at a typical chamber pressure of $<5 \times 10^{-5}$ Torr. In this work, a 10 nm layer (mass thickness, assumed density = 1.6 g/$cm^3$) of carbon film deposited from spectroscopically pure graphite (SPI Supplies, PA) was used as a covalent contact, followed by deposition of a 15 nm layer of Au as conducting leads. For carbon/molecule/Cu junctions, the e-C film was replaced by a 30 nm layer of Cu as top contact. Finally, microfabricated molecular junctions with either PPF substrate (Figure 3A) or e-C substrate (Figure 8B) were also used in this work. The fabrication process was detailed in our recent publication.[34] Throughout this Article, junctions are designated from bottom to top with layer thickness in nanometers in parentheses, for example, PPF/NAB(4.5)/e-C(10)/Au(15). Figure 1 shows a schematic of a carbon/molecule/carbon junction along with structures of molecules studied in this work.

*J*−*V* curves were collected at a scan rate of 100 V/s in air with a "4-wire" configuration (which corrects ohmic loss on both bottom and top electrodes), using a Labview-controlled data acquisition system, unless otherwise noted. Temperature experiments were performed in a Janis ST-500-1 cryogenic probe station cooled with liquid nitrogen. In all cases, the stated applied bias is bottom relative to the top electrode; therefore, a positive voltage means the bottom electrode is more positive than the top electrode, and positive current corresponds to electron flow from the top to the bottom electrodes.

## 3. RESULTS AND DISCUSSION

Before discussing the behavior of carbon/molecule/carbon molecular junctions, the properties of the PPF and e-C contact materials will be described. After the electronic results for the all-carbon junctions are presented, their properties are then compared to similar molecular junctions made with one metallic contact.

**3.1. Physical Properties of PPF and e-C.** PPF and e-C have been previously characterized by several analytical techniques including cyclic voltammetry (CV), X-ray photoelectron spectroscopy (XPS), atomic force microscopy (AFM), and Raman

**Table 1. Physical Properties of Freshly Prepared PPF and e-C Films**[a]

| film | resistivity[b] (Ω cm) | work function[c] (eV) | XPS surface O/C ratio (%) |
|---|---|---|---|
| PPF | 0.006 | 4.6 | 0.5 |
| e-C | 0.169 | 5.3 | 3.6 |

[a] Both PPF and e-C films were prepared on $SiO_2$/Si substrate, and the thicknesses are ~1 μm and 10 nm, respectively. [b] Resistivity values were obtained by four-probe electrical measurement. [c] Work functions were measured with a Kelvin probe instrument as previously described in ref 47.

spectroscopy.[48−51] It has been shown that both carbon films are disordered, conducting materials with electrochemical performance similar to that of glassy carbon. Furthermore, both films are exceedingly flat on a molecular scale with a typical root-mean-square (rms) roughness < 0.5 nm,[49,51] which is critical for fabrication of large-area molecular junctions with high yield and good reproducibility. However, there are significant differences in the physical and electronic properties of these two carbon materials that can impact junction behavior, as we will discuss below. Figure S1 in the Supporting Information shows Raman spectra of PPF and e-C films. Analysis of these spectra indicates that PPF is more ordered than e-C, but that both show signatures of disordered, $sp^2$-hybridized carbon. In addition, Figure S2 in the Supporting Information shows XPS spectra for freshly prepared PPF and e-C films. While both spectra show an asymmetric C1s peak centered at ~284 eV, characteristic of $sp^2$ carbon, e-C displays higher surface oxygen content (see Table 1).

The reduced order and increased surface oxygen content for e-C films would be expected to increase its electronic resistivity relative to that for PPF. The different physical characteristics can also lead to changes in other electronic properties of the material, such as work function. To provide a direct comparison of both materials, Table 1 lists the resistivity, work function, and XPS surface O/C ratio for freshly prepared PPF and e-C films. The resistivity of a 10 nm thick layer of e-C on $SiO_2$/Si is ~30 times higher than that for PPF. Using the values in Table 1 and the relationships for classical ohmic conduction, a 10 nm thick e-C top contact (area = 0.0017 $cm^2$) is predicted to have a resistance of $10^{-4}$ Ω along the direction of current flow (i.e., through a 10 nm length spread over a 0.0017 $cm^2$ area). This predicted series resistance of the e-C contact is negligible compared to the observed junction resistance, because the current path is through the short dimension (10 nm) of the e-C contact. An additional factor that can impact the conductance of molecular junctions is the work function of the contacts (i.e., due to energy level alignment; see, for example, refs 52−55). As noted in Table 1, the work function of e-C is higher than that of PPF by 0.7 eV. The work function difference can potentially be explained by the following two mechanisms, as previously proposed by Ago et al.:[56] (1) an increase of surface dipoles due to surface oxides (with positive poles close to the e-C surface); and (2) a reduced π-derived density of states (DOS) due to a reduction of π conjugation in the material. Both mechanisms are consistent with results from Raman and XPS characterization discussed above. Nevertheless, both PPF and e-C samples show exceedingly flat surfaces as revealed by AFM imaging. Collectively, the physical characterization of PPF and e-C demonstrates that both PPF and e-C are disordered carbon films with reasonable electrical conductivity and excellent surface flatness that are suitable as electrode materials for molecular electronics. In particular, the ability to deposit thin carbon films via electron beam evaporation makes it a good candidate as a top contact material. However, whenever directly depositing top contact materials onto "soft" molecular materials, it is important to evaluate if the deposition process causes damage to the molecular layer.

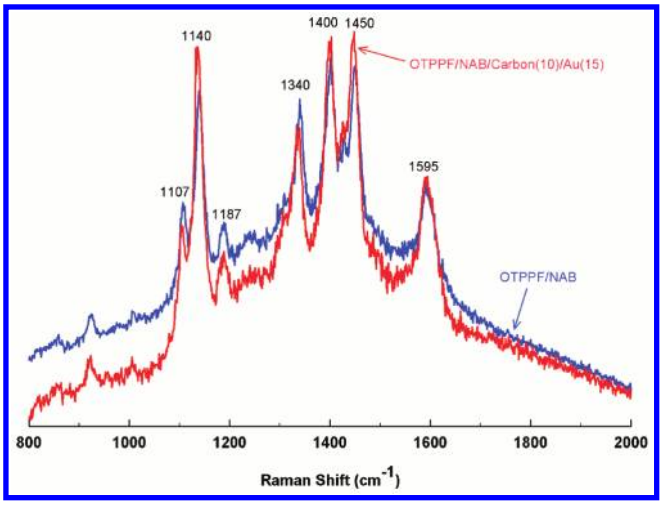


**Figure 2.** Raman spectra of NAB molecular layer on an optically transparent PPF (OTPPF) before (blue spectrum) and after deposition of a 10 nm layer of carbon and a 15 nm layer of Au (red spectrum).

**3.2. Structural Characterization after Carbon Deposition by Raman Spectroscopy.** To assess the integrity of molecules after carbon deposition, Raman spectra were collected before and after deposition of top contact materials, that is,10 nm e-C and 15 nm Au, on a 4.5 nm layer of NAB on optically transparent PPF (OTPPF) using a "backside" Raman probe described previously.[57] This technique enables spectroscopic characterization of the buried molecular layer and exploits the strong Raman signal obtained from the resonance-enhanced NAB molecules (at 514.5 nm). The deposition conditions were the same as those used to fabricate actual junctions, but the bottom carbon contact is ~10 nm thick (vs ~1 μm thick for typical PPF) to provide sufficient transparency.

Several Raman peaks associated with normal modes of the $-NO_2$ group, specifically, the phenyl$-NO_2$ stretch at 1107 $cm^{-1}$, the $-NO_2$ stretch at 1340 $cm^{-1}$, and the N═N vibration (coupled to the $-NO_2$ group) at 1450 $cm^{-1}$, serve as indicators of possible structural changes to the NAB molecules by direct evaporation of top contacts.[57−59] Figure 2 compares the Raman spectra of NAB molecules before and after carbon deposition. There is no change in the appearance or intensities of the NAB Raman bands, indicating that carbon deposition did not produce detectable structural changes in the NAB molecules. Therefore, no spectroscopic evidence indicates reaction of e-C with NAB or formation of covalent bonds between the molecular layer and the e-C. Similar results were obtained for Au deposition (see Figure S3 in the Supporting Information), as well as Cu and Ag deposition (spectra not shown). The lack of detectable damage to NAB is at least partially attributable to the strong covalent C−C bond (~4 eV) that anchors the molecular layer to substrate and the relative inertness of Au, Cu, and Ag metals. However, we have reported previously that significant decreases in the intensities of NAB Raman bands were observed upon Ti deposition, which

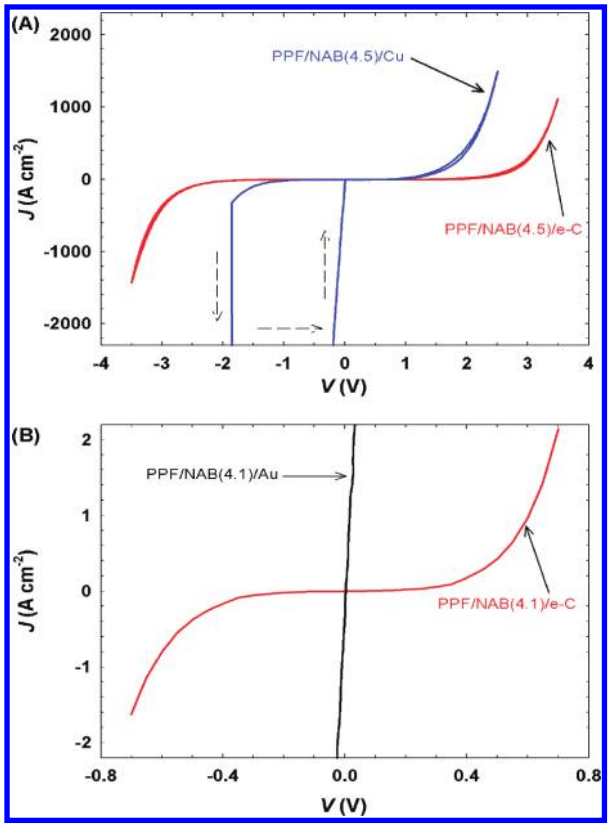


**Figure 3.** (A) Comparison of bias-stability of molecular junctions with Cu and e-C as top contacts. Cu junction broke down at ~ −1.86 V, due to electrochemical oxidation of Cu, while e-C is stable at least to a bias of ±3.5 V and current density up to ~1500 A/cm$^2$. The dotted arrows indicate the scan direction. Junction area: 15 $\mu$m × 15 $\mu$m = 225 $\mu$m$^2$. (B) Overlay of $J-V$ curves for PPF/NAB (4.1)/Au junctions with and without a 10 nm layer of e-C between NAB and Au. The e-C film acts as a barrier layer to prevent Au penetration.

was attributed to the reaction of Ti and the terminal $-NO_2$ group and formation of a Ti−N bond between Ti and NAB.[58,59] Other investigators have also reported that vapor-deposited Ti results in complete destruction of conjugated self-assembled monolayers (SAMs) on Au.[30] Additionally, it is worth noting that, although Raman spectroscopy provides structural information about the molecular layer, it cannot reveal whether there is physical penetration or diffusion of vapor-deposited metal atoms into the molecular layer, which can greatly affect electronic characteristics of molecular junctions, as discussed in the next section.

**3.3. Importance of Carbon as a Covalent Contact.** As noted in the Introduction, PPF/molecule/metal molecular junctions may be fabricated reproducibly, but the metal is susceptible to electromigration or oxidation. The blue curve in Figure 3A shows the breakdown of a PPF/NAB(4.5)/Cu junction at ~ −1.86 V bias (when Cu is positively biased) and ~300 A cm$^{-2}$, indicated by the dramatic and irreversible increase in junction conductance. This behavior was previously attributed to the electrochemical oxidation of Cu metal, resulting in the formation of copper cations, which undergo electromigration under the applied electric field, then are reduced at the PPF electrode to form Cu filaments.[35] A similar process has been exploited to make nonvolatile memory devices containing $Cu^+$ or $Ag^+$ conducting solid electrolytes, by reversibly forming and oxidizing metal filaments.[60−62] The red curve in Figure 3A shows that when both the bottom and the top electrodes are composed of carbon materials, the junction can be swept to at least ±3.5 V and ~1500 A cm$^{-2}$, without breakdown. The enhanced stability of all-carbon molecular devices to bias stress is likely due to the difficulty of oxidation or electromigration of both PPF and e-C as compared to most metals. Because carbon is a covalent conductor, migration of carbon requires breaking strong C−C bonds (~4 eV). On the other hand, it is well-known in the semiconductor industry that electromigration of metal interconnects can lead to eventual device failure, which is exacerbated by high current densities and high temperatures with increasing device miniaturization.[63] Although an inert metal such as gold might resist the reactions associated with bias-driven filament formation, we have found that it is much more difficult to form molecular junctions with direct deposition of Au onto diazonium-derived molecular layers. Figure 3B shows that deposition of Au onto PPF/NAB (4.1) results in electrical short-circuits, while a 10 nm layer of e-C between NAB and Au is sufficient to prevent "shorts" between the PPF and top contact materials. Recalling that the Raman spectra of the NAB layer before and after Au deposition indicate no apparent structural changes in the NAB layer (Figure S3), these results imply that electrical shorts are not caused by structural changes in NAB, but instead by Au penetration into and/or completely through the molecular layer as was previously reported by other researchers.[27,30,31,38,64] As shown in the Supporting Information (Figure S4), devices made using a 1 nm (mass thickness) layer of e-C between NAB and Au displayed characteristics similar to those with no e-C film, while junctions made using e-C film thicknesses between 2 and 30 nm showed statistically indistinguishable nonlinear $J-V$ responses. These results indicate that e-C can effectively act as a barrier to prevent Au from penetrating into the molecular layer once the e-C film thickness increases beyond a threshold value. Thus, the role of the e-C film is similar to that of the PEDOT:PSS conducting polymer layer used by Akkerman et al.[16] for fabrication of large-area molecular junctions, or the $Al_2O_3$ layer formed by atomic layer deposition (ALD) reported by Preiner and Melosh,[39] but with the convenience of direct e-beam deposition. Furthermore, the e-C layer provides a more symmetric carbon/molecule/carbon device, with the composition of the two contacting layers being similarly disordered but conductive $sp^2$ carbon.

**3.4. Device Yield and Reproducibility.** Figure 4A shows an overlay of 32 $J-V$ curves of PPF/NAB (4.5)/e-C(10)/Au (15) junctions from four independently fabricated chips having eight junctions each, with the averaged $J-V$ curve for each batch plotted on a semilog scale in Figure 4B. The relative standard deviation (rsd) of the low voltage resistance (LVR) is typically 10−30%, and the rsd of $J$ at ±0.5 V is 10−20%, as summarized in Table S1 of the Supporting Information. Device yield, defined as the percentage of devices that were not "shorted", was 100% for each of the four batches included in Figure 4B and rarely was below 80% for all devices made with e-C(10)/Au as the top contact. Overall, junctions fabricated with e-C as top contact show high yield and good reproducibility, which are important prerequisites for not only studying charge transport mechanisms but also for possible commercial applications.

**3.5. Junction Characteristics and Charge Transport Mechanism.** To investigate the charge transport mechanism in carbon/molecule/carbon junctions, the molecular layer thickness and structure were varied, and the temperature dependence of the current was determined. Figure 5A shows $J-V$ curves on a

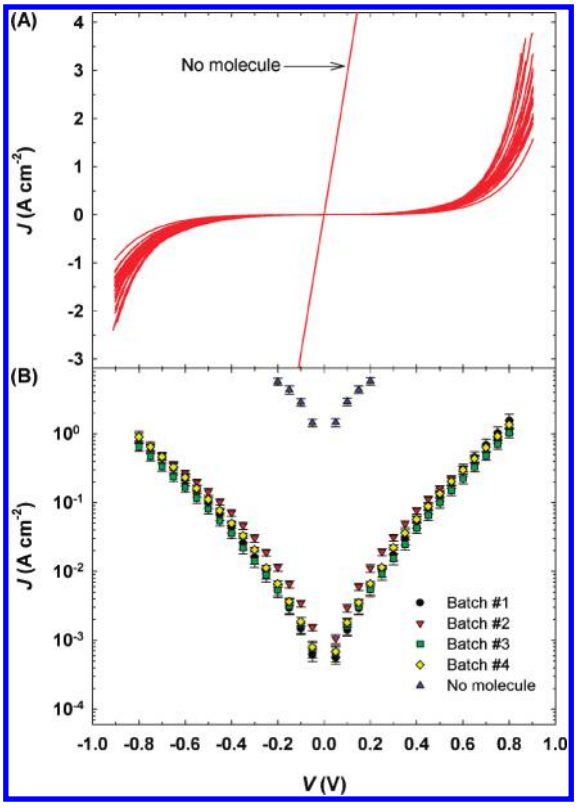


**Figure 4.** Overlay of $J-V$ curves for 32 PPF/NAB (4.5)/e-C/Au junctions from four different batches for linear (A) and semilog (B) scales. The yield is 100% (32/32), and the relative standard deviation (rsd) of $J$ at ±0.5 V is 10−20%. The error bars represent ±1 standard deviation. "No molecule" curves were obtained with PPF/e-C/Au devices with no molecular layer.

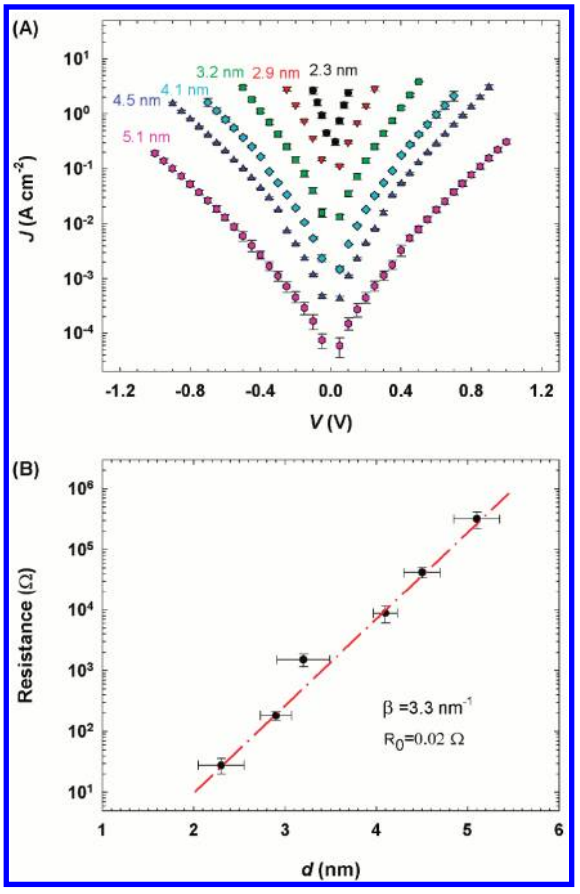


**Figure 5.** (A) $J-V$ curves for PPF/NAB/e-C/Au junctions as a function of NAB thickness. (B) Attenuation plot constructed from the low voltage resistances, yielding an attenuation factor $\beta = 3.3$ nm$^{-1}$ and contact resistance $R_o = 0.02$ Ω. Each data point represents the average of all eight junctions on each sample. Error bars represent ±1 standard deviation unit, for both layer thickness and observed resistance. Table S3 in the Supporting Information lists the individual low-voltage resistance values for all 48 devices.

semilog scale for PPF/NAB/e-C junctions as a function of NAB thickness in the range of 2.3−5.1 nm. Each $J-V$ curve is an average of four junctions across a single e-C/Au stripe on the same sample. Regardless of molecular thickness, all $J-V$ curves show a similar shape, with a linear increase in $J$ at low voltage ($V = \pm 0.1$ V) and an exponential increase in $J$ at higher bias, implying a tunneling mechanism. Figure 5B shows an attenuation plot, $\ln(R)$ versus molecular thickness ($R$ is the low voltage resistance determined by the inverse slope of linear $I-V$ fitting for $V = \pm 0.1$ V). The attenuation plot clearly shows that low-voltage junction resistance is an exponential function of molecular thickness, consistent with an expression derived for non-resonant tunneling transport:[53,65,66]

$$R = R_0 \exp(\beta d)$$

where $R_0$ is the contact resistance, $\beta$ is the attenuation factor, and $d$ is molecular thickness. The attenuation factor, $\beta$, determined from the slope of the plot, is 3.3 nm$^{-1}$, slightly larger than the value obtained for junctions with Cu as top contact, which yielded 2.5 nm$^{-1}$,[33] but similar to that observed for other conjugated molecular junctions.[67,68] In addition to $\beta$, the specific contact resistance $R_c$ (obtained by multiplying contact resistance $R_c$ by junction area) can be determined from the $y$-axis intercept of the plot in Figure 5B by extrapolating to zero molecular thickness. This yields a specific contact resistance value of $3.4 \times 10^{-5}$ Ω cm$^2$. By comparison, the recently reported value[33] for PPF/NAB/Cu junctions is $6.5 \times 10^{-4}$ Ω cm$^2$, which is ∼20 times larger than that of analogous e-C junctions. For comparison to molecular junctions with metallic contacts, a specific contact resistance of $5.8 \times 10^{-9}$ Ω cm$^2$ was reported for Au/alkylmonothiol/Au junctions,[54] a value of $3.4 \times 10^{-5}$ Ω cm$^2$ for large-area Au/*para*-phenylenethiol/PEDOT:PSS/Au junctions,[69] and $1.3 \times 10^{-10}$ Ω cm$^2$ and ∼$10^{-9}$ Ω cm$^2$ for conducting-probe AFM-based Au/oligoacenethiol/Au and Au/alkylmonothiol/Au molecular junctions (assuming a junction area of 10 nm$^2$ for an AFM tip radius of ∼50 nm).[65,70] Frisbie et al. have attributed variations in contact resistance to the relationship between the contact Fermi level and molecular orbital energies,[53,70] but other factors may be involved, such as the actual contacting area, contact roughness, and variations of interfacial bonding and physisorption geometry.

Figure 6A shows $J-V$ curves for PPF/NAB(4.5)/e-C(10)/Au(15) junctions at several temperatures between 100 and 400 K. Figure 6B shows the corresponding Arrhenius plot of $\ln(J)$ versus $1000/T$ for three bias voltages. A similar temperature dependence was observed for carbon/molecule/Cu junctions,[33] where it was shown to be consistent with quantum mechanical tunneling over the entire temperature range considered. The apparent increase in slope, to 40−60 meV above 200 K, was

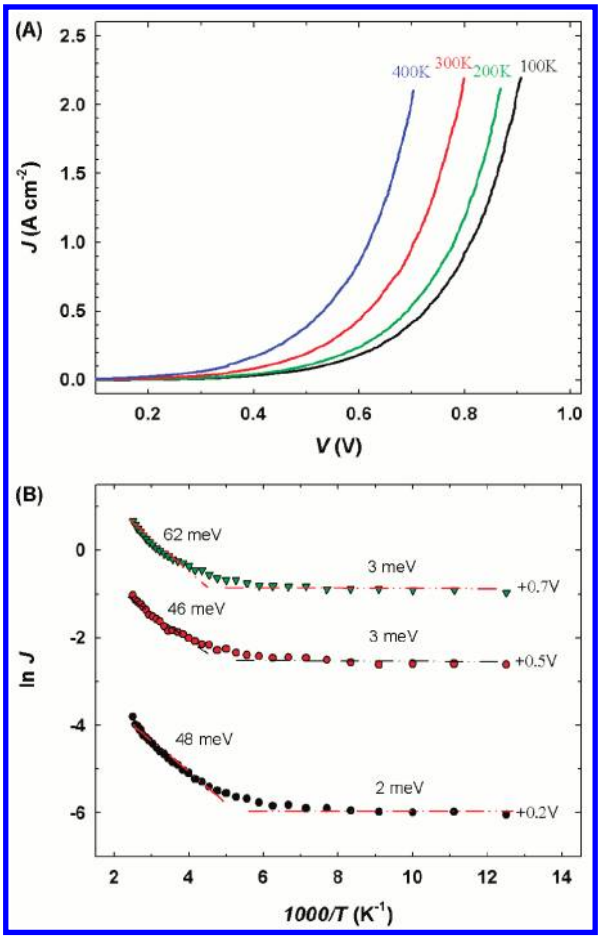


**Figure 6.** (A) $J-V$ curves for PPF/NAB(4.5)/e-C junctions at selected temperatures from 100 to 400 K. (B) Arrhenius plots at different junction biases. The activation energies calculated from the plot are 46−62 meV for the 200−400 K temperature range and 2−3 meV for the 100−200 K temperature range.

attributed to broadening of the electron Fermi function distribution in the contacts at elevated temperatures. Thus, no thermally activated process in the molecular layer is required to account for the observed temperature dependence. We note that junctions containing different molecular layers [FL(2.5) and $C_8N$(2.3)] show qualitatively similar temperature dependence (see Figure S5 in the Supporting Information). Therefore, the temperature-dependent $J-V$ measurements support the conclusion that nonresonant tunneling is the dominant charge transport mechanism for PPF/molecule/e-C junctions, as well as for the previously reported PPF/molecule/Cu devices.[15,32−34]

The effect of molecular structure on transport through quantum mechanical tunneling can be evaluated by considering the energy alignment between molecular orbitals and the electrode Fermi level. Figure 7 shows an overlay of $J-V$ curves for PPF/molecule/e-C junctions fabricated with three different molecular layers with similar thicknesses: NAB (2.3), FL (2.5), and $C_8N$ (2.3). The low voltage resistances (LVR, $V = \pm 0.1$ V) for these junctions are 35(±4), 931(±40), and 3390(±130) Ω, respectively. Thus, for the same molecular thickness of 2.3−2.5 nm, the current density for junctions with a conjugated NAB layer is roughly 2 orders of magnitude higher than that for an aliphatic $C_8N$ layer. Thus, Figure 7 clearly shows that junction conductance has a strong dependence on molecular structure. However, it is not yet clear which aspects of molecular structure are most important for controlling junction conductance.

It is generally believed that the energy level offset between the electrode Fermi level and the frontier molecular orbitals is most important in determining the tunneling barrier in metal/molecule/metal devices; therefore, the frontier orbital energy is expected to exert a strong influence on junction conductance.[71−74] We reported previously that the molecular HOMO energy is generally closer to the electrode Fermi level for diazonium derived molecular layers than the LUMO.[33] Table 2 lists the energy levels of the molecular orbitals determined using density functional theory (DFT) (Gaussian 03, DFT/B3LYP method with 6-31G (d) basis set) for gas-phase molecular dimers with lengths close to the layer

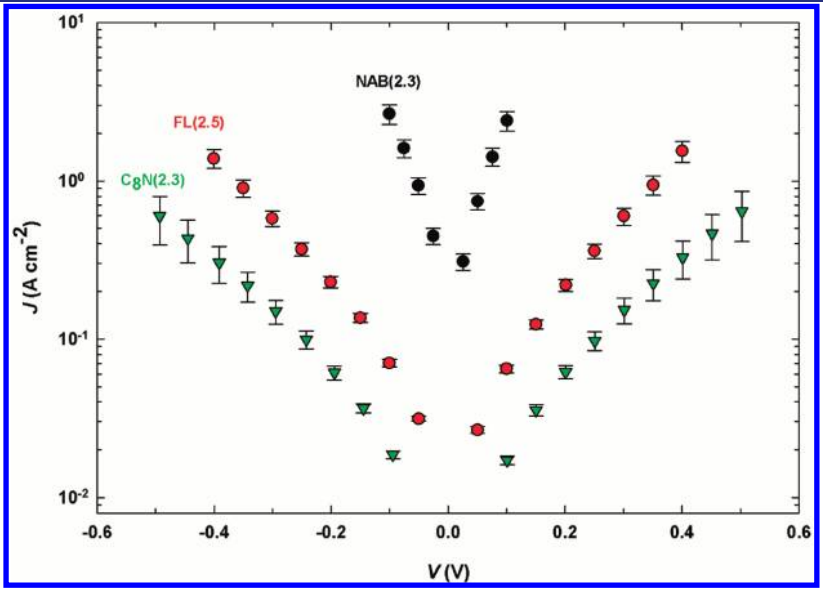


**Figure 7.** Overlay of $J-V$ curves for PPF/molecule/e-C junctions fabricated with three different molecular layers with similar thickness: NAB (2.3 nm), FL (2.5 nm), and $C_8N$ (2.3 nm).

**Table 2. Molecular Energy Levels and Tunneling Barriers from Density Functional Theory (DFT), Ultraviolet Photoelectron Spectroscopy (UPS), or Simmons Fitting (Unit: eV)**

| molecule | HOMO[a] | LUMO[a] | energy gap[a] | $E_f - E_{homo}$ from DFT[b] | $E_f - E_{homo}$ from UPS[c] | tunneling barrier, $\Phi$[d] |
|---|---|---|---|---|---|---|
| NAB | −6.61 | −3.64 | 2.97 | 2.01 | 1.16 | 1.13 |
| FL | −5.25 | −1.33 | 3.92 | 0.65 | 1.52 | 1.31 |
| $C_8N$ | −6.21 | 1.99 | 8.20 | 1.61 | 1.96 | 1.75 |

[a] HOMO and LUMO energies were calculated by Gaussian 03 for gas-phase molecular dimers, using the DFT/B3LYP method with a 6-31G (d) basis set. Energy gap is the energy level difference between HOMO and LUMO. [b] $E_f$ corresponds to the negative value of the experimental work function of PPF (−4.6 eV) measured by Kelvin probe. [c] $E_f - E_{homo}$ was determined from the onset of photoemission in UPS spectra. See the Supporting Information for details. [d] Tunneling barrier, $\Phi$, was obtained by fitting experimental data in Figure 7 to the Simmons model with image charge and effective mass effects included as descried in ref 33.

thicknesses indicated in Figure 7 and the resulting barrier height ($E_f - E_{HOMO}$). Also included in Table 2 are $E_f - E_{HOMO}$ determined for molecular layers bonded to PPF using ultraviolet photoelectron spectroscopy (UPS), as well as apparent barrier heights determined by fitting experimental data to the Simmons model. A correlation between junction conductance and $E_f - E_{HOMO}$ predicted from DFT for either the molecular monomers or the dimers is not apparent. This is possibly due to the fact that DFT calculations of molecular orbitals are based on isolated gas-phase molecules instead of the complete electrode−molecule system, where several factors can affect the electrode−molecule interfacial energetics. For example, electrode−molecule interactions,[75−77] molecular dipole effects,[78,79] and image charge effects[33,80] are not reflected in the gas-phase calculations. Particularly for the case of a covalent substrate−molecule bond, the C−C or C−N surface bond can potentially result in strong electrode−molecule electronic coupling and significantly altered interfacial energetics at the electrode−molecule interface.[81]

Interfacial energetics of the PPF/molecule interface were further investigated with ultraviolet photoelectron spectroscopy (UPS), as it can provide direct measurements of the work function of the substrate and the HOMO onset energy, which is closely related to the tunneling barrier. Figure S6 in the Supporting Information shows the UPS spectra of PPF substrates with and without the three molecular layers (NAB, FL, and $C_8N$). The values for $E_{HOMO}$ were determined from the onset of photoemission with respect to the electrode Fermi energy and are listed in Table 2. The $E_f - E_{HOMO}$ values determined from UPS[82] are 1.16, 1.52, and 1.96 eV for NAB, FL, and $C_8N$ molecular layers on PPF, respectively, and these follow the trend of junction conductance in Figure 7, with smaller $E_f - E_{HOMO}$ corresponding to higher junction conductance. Qualitative correlations between energy level alignment and junction conductance have been previously reported in both experimental and theoretical reports.[73,74,83] However, a quantitative and precise correlation between junction conductance and energy level alignment[84−86] will require additional investigations and a more detailed understanding of several parameters that relate to molecular structure, electrode−molecule coupling, intermolecular interactions, etc. A more detailed theoretical analysis using the nonequilibrium Green's function approach[87−91] is currently in progress.

**3.6. Effect of Electrode Materials on Junction Conductance.** Figure 8A shows a direct comparison of the $J-V$ curves for molecular junctions containing a 4.5 nm layer of NAB on PPF with two different top electrode materials: Cu and e-C. The increased conductance of the Cu top contact device can be assessed by considering the current density at 0.2 V, which is a factor of ~7.3 times that for the e-C top contact junction. Figure 8B presents a similar comparison for junctions with e-C as the top contact and PPF and e-C as substrates. In this case, the e-C bottom contact junction is more than 1 order of magnitude less conductive than that with PPF as bottom contact (by comparing current densities at the same bias). XPS surface analysis shows that the atomic surface concentration of nitrogen is similar for the NAB layer on PPF and e-C, which implies that the packing densities of the NAB layers on PPF and e-C are similar. Therefore, the difference in junction conductance is not due to variation of the coverage and thickness of the molecular layer but rather to the difference in contact materials. We have fit these data to the Simmons model to determine the apparent barrier height, $\Phi_B$,

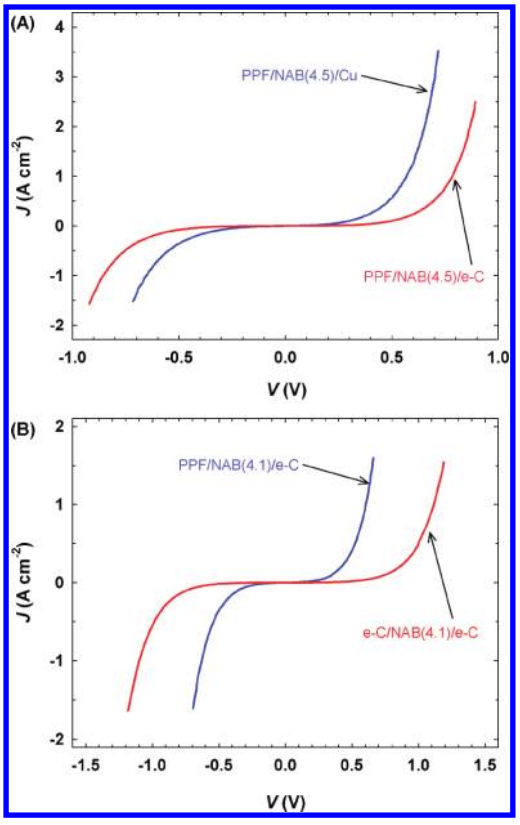


**Figure 8.** Effect of electrode materials on junction conductance. (A) Comparison of top contact materials: Cu versus e-C. (B) Comparison of bottom contact materials: PPF versus e-C. The barrier heights determined from fitting the data to the Simmons model are 1.19 eV for PPF/NAB(4.5)/e-C, 1.06 eV for PPF/NAB(4.5)/Cu, 1.16 eV for PPF/NAB(4.1)/e-C, and 1.38 eV for e-C/NAB(4.1)/e-C.

yielding barriers of 1.06 eV for PPF/NAB(4.5)/Cu and 1.19 eV for PPF/NAB(4.5)/e-C. For junctions in Figure 8B, e-C/NAB(4.1)/e-C was fit well with $\Phi_B$ = 1.38 eV, while PPF/NAB (4.1)/e-C was best fit with $\Phi_B$ = 1.16 eV. With these apparent barrier heights, we have also semiquantitatively analyzed the results in Figure 8 within the Landauer limit (see analysis in the Supporting Information). We found that coupling strength between NAB molecules and electrodes alone cannot adequately explain the results in Figure 8. Therefore, an alternative explanation is needed.

The differences in conductance between PPF/NAB/Cu and PPF/NAB/e-C junctions in Figure 8A and between PPF/NAB/e-C and e-C/NAB/e-C junctions in Figure 8B can be explained by differences in the surface density of states(DOS) in the electrode materials, as suggested by several theoretical calculations.[92−94] Disordered carbon materials are known to have a lower density of states at the Fermi energy than that of metals;[95] that is, Cu has higher surface density of states than e-C or PPF. On the other hand, a reduced graphitic structure (or less $sp^2$ fraction) in e-C can possibly lead to lower surface density of electronic states than PPF, resulting in a decreased charge carrier density in the electrode, and therefore lower junction conductance. Arena et al.[96] and Koivusaari et al.[97] have studied surface density of states of tetrahedral amorphous carbon by scanning tunneling spectroscopy (STS). In this technique, density of states can be derived from normalized differential conductivity, which is proportional to DOS. Their results showed that an increased density of surface $\pi$ states was resulted from $sp^2$-rich graphitic bonding on the surface as compared to that in the bulk. This conclusion is also consistent with the proposal by Ago et al.[56] that a reduction in $\pi$ conjugation lowers the $\pi$-derived DOS, as mentioned earlier. Furthermore, PPF is formed at 1000 °C for 1 h, while e-C is formed by deposition on a room temperature substrate and is only briefly subjected to elevated temperatures during deposition. We reported previously that annealing of e-C significantly decreases its resistivity and increases its electrochemical reactivity, which are both indications of a higher surface density of electronic states.[51] Overall, results in Figure 8 indicate that electronic properties of the electrode materials can have a significant impact on junction conductance.

**3.7. Thermal Stability and Cycle Life.** Practical application of molecular electronic devices will require not only high device yield and reproducibility, but also temperature stability and long cycle life. We have recently demonstrated that, although the NAB molecular layer covalently bonded to a carbon substrate can survive temperatures up to 400 °C in a vacuum (probed by Raman spectroscopy before and after heat treatment), finished carbon/NAB/Cu junctions can only withstand temperatures up to ~200 °C for 5 min in a vacuum without significant changes in $J-V$ behavior.[98] At higher temperatures, junction conductance increased, in one case, by a factor of 33 (at $V$ = 0.2 V) for a sample heated to 400 °C. The increase in junction conductance was attributed to possible penetration of Cu atoms into the molecular layer due to thermally induced migration at higher temperatures.[98] Figure 9 shows results from similar experiments performed on finished carbon/NAB/carbon molecular junctions but with longer heat treatment time. As shown, the all-carbon devices can withstand temperatures at least up to 300 °C for 30 min with minimal change in electronic behavior. Even at 400 °C, current at 0.2 V was only increased by a factor of ~4 for these all-carbon junctions. The significantly improved thermal stability of all-carbon devices is most likely due to the nature of carbon as a covalent material, which can "block" migration of metal atoms at

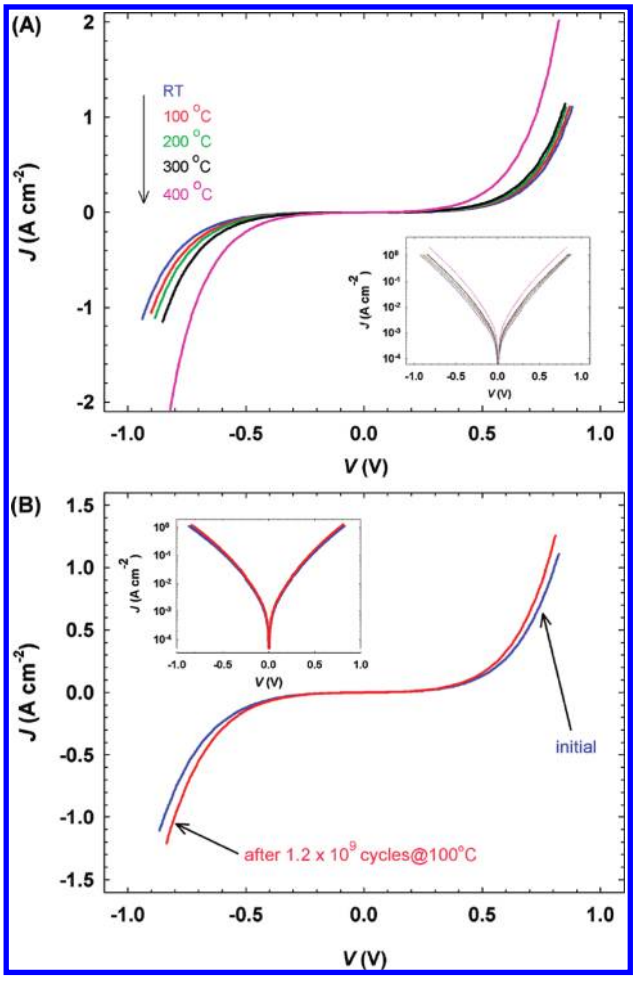


**Figure 9.** (A) $J-V$ curves of a PPF/NAB(4.5)/e-C junction heated in a vacuum ($2-4 \times 10^{-6}$ Torr) at progressively elevated temperatures for 30 min at each temperature. Each $J-V$ curve was taken in lab ambient after the sample was cooled to room temperature. (B) $J-V$ curves of a PPF/NAB(4.5)/e-C junction before and after triangle wave (±1 V, 5 kHz) cycling up to $1.2 \times 10^9$ cycles at 100 °C over the course of ~68 h in air. The insets display the same data plotted in a semilog scale.

elevated temperatures. This thermal stability is well beyond that of most finished molecular electronic devices reported to date, ensuring that all-carbon molecular devices can be readily compatible with high-temperature (up to 400 °C) processing steps required by current semiconductor technology.[99]

To test cycle life, a finished carbon/NAB/carbon junction was cycled with a triangle wave (±1 V, 5 kHz) at 100 °C in lab ambient. The junction was scanned at least up to $1.2 \times 10^9$ cycles under these conditions without significant change in $J-V$ characteristics, as shown in Figure 9B. Overall, these tests show that as-fabricated all-carbon molecular junctions have excellent thermal stability and robustness, which makes them readily compatible with current microelectronic processing and potential real-world operation.

## 4. CONCLUSIONS

We have shown that all-carbon molecular junctions can be fabricated by electron beam evaporation of a carbon top contact onto molecular layers covalently bonded to a carbon substrate with high yield, excellent reproducibility, and enhanced bias and

thermal stability. The fact that both the substrate and the top contact are covalent conductors results in greater stability and lower tendency for electromigration in carbon/molecule/carbon devices as compared to similar structures containing metals. Electronic characterization showed that nonresonant tunneling is likely the dominant charge transport mechanism, in agreement with previous results for Cu and Au top contact devices. In addition, it was shown that junction conductance depends on molecular structure. Ultraviolet photoemission spectroscopy (UPS) was employed to determine the energy level offsets between the molecular HOMO ($E_{homo}$) and the electrode Fermi level ($E_f$). Junction conductance qualitatively correlates with UPS measurements in that lower $E_f - E_{homo}$ offset corresponding to higher conductance. These energy level offsets were similar to tunneling barriers obtained by fitting the experimental data to the Simmons model, implying that charge transport through these junctions are mediated by molecular HOMOs. Furthermore, junction conductance was also shown to depend on electrode materials, possibly due to variation of the electronic density of states of the substrate and top contact. Collectively, these results indicate that use of covalent contacts for molecular electronics provides a reliable means to fabricate robust devices viable for charge transport studies, as well as for future integration and practical applications.

## ■ ASSOCIATED CONTENT

**Supporting Information.** Experimental details for Raman spectroscopy, ultraviolet photoelectron spectroscopy (UPS), and X-ray photoelectron spectroscopy (XPS); data analysis in Figure 8 within the Landauer limit; and supporting figures and tables. This material is available free of charge via the Internet at http://pubs.acs.org.

## ■ AUTHOR INFORMATION

**Corresponding Author**
richard.mccreery@ualberta.ca

## ■ ACKNOWLEDGMENT

This work was supported by the Natural Sciences and Engineering Research Council of Canada, the National Institute for Nanotechnology, the University of Alberta, and the Alberta Ingenuity Fund. We would like to acknowledge Amr Mahmoud for assistance with Raman spectroscopy, Jie Ru and Nikola Pekas for providing microfabricated substrates, Bryan Szeto for technical assistance, and Dr. Shihong Xu in the Alberta Centre for Surface Engineering and Science (ACSES) at the University of Alberta for collecting XPS and UPS spectra.

## ■ REFERENCES

(1) Heath, J. R.; Ratner, M. A. *Phys. Today* **2003**, *56*, 43–49.
(2) McCreery, R. L. *Chem. Mater.* **2004**, *16*, 4477–4496.
(3) Tao, N. J. *Nat. Nanotechnol.* **2006**, *1*, 173–181.
(4) Heath, J. R. *Annu. Rev. Mater. Res.* **2009**, *39*, 1–23.
(5) McCreery, R. L.; Bergren, A. J. *Adv. Mater.* **2009**, *21*, 1–20.
(6) Akkerman, H. B.; de Boer, B. *J. Phys.: Condens. Matter* **2008**, *20*, 013001.
(7) Kim, W. Y.; Choi, Y. C.; Min, S. K.; Cho, Y.; Kim, K. S. *Chem. Soc. Rev.* **2009**, *38*, 2319–2333.
(8) Feldman, A. K.; Steigerwald, M. L.; Guo, X.; Nuckolls, C. *Acc. Chem. Res.* **2008**, *41*, 1731–1741.
(9) Reed, M. A.; Zhou, C.; Muller, C. J.; Burgin, T. P.; Tour, J. M. *Science* **1997**, *278*, 252.
(10) Wold, D. J.; Frisbie, C. D. *J. Am. Chem. Soc.* **2001**, *123*, 5549–5556.
(11) Cui, X. D.; Primak, A.; Zarate, X.; Tomfohr, J.; Sankey, O. F.; Moore, A. L.; Moore, T. A.; Gust, D.; Harris, G.; Lindsay, S. M. *Science* **2001**, *294*, 571–574.
(12) Xu, B.; Tao, N. J. *Science* **2003**, *301*, 1221–1223.
(13) Kushmerick, J. G.; Holt, D. B.; Yang, J. C.; Naciri, J.; Moore, M. H.; Shashidhar, R. *Phys. Rev. Lett.* **2002**, *89*, 086802.
(14) Holmlin, R. E.; Haag, R.; Chabinyc, M. L.; Ismagilov, R. F.; Cohen, A. E.; Terfort, A.; Rampi, M. A.; Whitesides, G. M. *J. Am. Chem. Soc.* **2001**, *123*, 5075–5085.
(15) Anariba, F.; Steach, J. K.; McCreery, R. *J. Phys. Chem. B* **2005**, *109*, 11163–11172.
(16) Akkerman, H. B.; Blom, P. W. M.; de Leeuw, D. M.; de Boer, B. *Nature* **2006**, *441*, 69.
(17) Anariba, F.; McCreery, R. L. *J. Phys. Chem. B* **2002**, *106*, 10355–10362.
(18) Chiechi, R. C.; Weiss, E. A.; Dickey, M. D.; Whitesides, G. M. *Angew. Chem., Int. Ed.* **2008**, *47*, 142–144.
(19) Metzger, R. M.; Xu, T.; Peterson, I. R. *J. Phys. Chem. B* **2001**, *105*, 7280–7290.
(20) Haick, H.; Niitsoo, O.; Ghabboun, J.; Cahen, D. *J. Phys. Chem. C* **2007**, *111*, 2318–2329.
(21) Vilan, A.; Cahen, D. *Adv. Funct. Mater.* **2002**, *12*, 795–807.
(22) Shimizu, K. T.; Fabbri, J. D.; Jelincic, J. J.; Melosh, N. A. *Adv. Mater.* **2006**, *18*, 1499–1504.
(23) Loo, Y.-L.; Lang, D. V.; Rogers, J. A.; Hsu, J. W. P. *Nano Lett.* **2003**, *3*, 913–917.
(24) Collier, C. P.; Jeppesen, J. O.; Luo, Y.; Perkins, J.; Wong, E. W.; Heath, J. R.; Stoddart, J. F. *J. Am. Chem. Soc.* **2001**, *123*, 12632–12641.
(25) Stewart, D. R.; Ohlberg, D. A. A.; Beck, P. A.; Chen, Y.; Williams, R. S.; Jeppesen, J. O.; Nielsen, K. A.; Stoddart, J. F. *Nano Lett.* **2004**, *4*, 133–136.
(26) Walker, A. V.; Tighe, T. B.; Cabarcos, O. M.; Reinard, M. D.; Haynie, B. C.; Uppili, S.; Winograd, N.; Allara, D. L. *J. Am. Chem. Soc.* **2004**, *126*, 3954–3963.
(27) Walker, A. V.; Tighe, T. B.; Stapleton, J.; Haynie, B. C.; Upilli, S.; Allara, D. L.; Winograd, N. *Appl. Phys. Lett.* **2004**, *84*, 4008–4010.
(28) Zhu, Z.; Daniel, T. A.; Maitani, M.; Cabarcos, O. M.; Allara, D. L.; Winograd, N. *J. Am. Chem. Soc.* **2006**, *128*, 13710–13719.
(29) Jiang, W.; Zhitenev, N.; Bao, Z.; Meng, H.; Abusch-Magder, D.; Tennant, D.; Garfunkel, E. *Langmuir* **2005**, *21*, 8751–8757.
(30) de Boer, B.; Frank, M. M.; Chabal, Y. J.; Jiang, W.; Garfunkel, E.; Bao, Z. *Langmuir* **2004**, *20*, 1539–1542.
(31) Kim, T.-W.; Wang, G.; Lee, H.; Lee, T. *Nanotechnology* **2007**, *18*, 315204.
(32) Bergren, A. J.; Harris, K. D.; Deng, F.; McCreery, R. L. *J. Phys.: Condens. Matter* **2008**, *20*, 374117.
(33) Bergren, A. J.; McCreery, R. L.; Stoyanov, S. R.; Gusarov, S.; Kovalenko, A. *J. Phys. Chem. C* **2010**, *114*, 15806–15815.
(34) Ru, J.; Szeto, B.; Bonifas, A.; McCreery, R. L. *ACS Appl. Mater. Interfaces* **2010**, *2*, 3693–3701.
(35) Ssenyange, S.; Yan, H.; McCreery, R. L. *Langmuir* **2006**, *22*, 10689–10696.
(36) Schindler, C.; Thermadam, S. C. P.; Waser, R.; Kozicki, M. N. *IEEE Trans. Electron Devices* **2007**, *54*, 2762–2768.
(37) Banno, N.; Sakamoto, T.; Iguchi, N.; Sunamura, H.; Terabe, K.; Hasegawa, T.; Aono, M. *IEEE Trans. Electron Devices* **2008**, *55*, 3283–3287.
(38) Kuikka, M. A.; Li, W.; Kavanagh, K. L.; Yu, H.-Z. *J. Phys. Chem. C* **2008**, *112*, 9081–9088.
(39) Preiner, M. J.; Melosh, N. A. *Appl. Phys. Lett.* **2008**, *92*, 213301.
(40) Bonifas, A. P.; McCreery, R. L. *Nat. Nanotechnol.* **2010**, *5*, 612–617.
(41) Avouris, P.; Chen, Z.; Perebeinos, V. *Nat. Nanotechnol.* **2007**, *2*, 605–615.

(42) Yao, Z.; Postma, H. W. C.; Balents, L.; Dekker, C. *Nature* **1999**, *402*, 273–276.
(43) Li, X.; Wang, X.; Zhang, L.; Lee, S.; Dai, H. *Science* **2008**, *319*, 1229–1232.
(44) Martin, C. A.; Ding, D.; Sorensen, J. K.; Bjornholm, T.; van Ruitenbeek, J. M.; van der Zant, H. S. J. *J. Am. Chem. Soc.* **2008**, *130*, 13198–13199.
(45) Borrnert, F.; et al. *Phys. Rev. B* **2010**, *81*, 085439.
(46) Ranganathan, S.; Steidel, I.; Anariba, F.; McCreery, R. L. *Nano Lett.* **2001**, *1*, 491–494.
(47) Yan, H.; McCreery, R. L. *ACS Appl. Mater. Interfaces* **2009**, *1*, 443–451.
(48) Ranganathan, S.; McCreery, R.; Majji, S. M.; Madou, M. *J. Electrochem. Soc.* **2000**, *147*, 277–282.
(49) Ranganathan, S.; McCreery, R. L. *Anal. Chem.* **2001**, *73*, 893–900.
(50) Anariba, F.; DuVall, S. H.; McCreery, R. L. *Anal. Chem.* **2003**, *75*, 3837–3844.
(51) Blackstock, J. J.; Rostami, A. A.; Nowak, A. M.; McCreery, R. L.; Freeman, M. R.; McDermott, M. T. *Anal. Chem.* **2004**, *76*, 2544–2552.
(52) Beebe, J. M.; Engelkes, V. B.; Miller, L. L.; Frisbie, C. D. *J. Am. Chem. Soc.* **2002**, *124*, 11268–11269.
(53) Engelkes, V. B.; Beebe, J. M.; Frisbie, C. D. *J. Am. Chem. Soc.* **2004**, *126*, 14287–14296.
(54) Wang, G.; Kim, T.-W.; Jang, Y. H.; Lee, T. *J. Phys. Chem. C* **2008**, *112*, 13010–13016.
(55) Rauba, J. M. C.; Strange, M.; Thygesen, K. S. *Phys. Rev. B* **2008**, *78*, 165116.
(56) Ago, H.; Kugler, T.; Cacialli, F.; Salaneck, W. R.; Shaffer, M. S. P.; Windle, A. H.; Friend, R. H. *J. Phys. Chem. B* **1999**, *103*, 8116–8121.
(57) Mahmoud, A. M.; Bergren, A. J.; McCreery, R. L. *Anal. Chem.* **2009**, *81*, 6972–6980.
(58) Nowak, A.; McCreery, R. *J. Am. Chem. Soc.* **2004**, *126*, 16621–16631.
(59) Nowak, A. M.; McCreery, R. L. *Anal. Chem.* **2004**, *76*, 1089–1097.
(60) Kozicki, M. N.; Mitkova, M.; Aberouette, J. P. *Physica E* **2003**, *19*, 161–166.
(61) Kozicki, M. N.; Mitkova, M.; Park, M.; Balakrishnan, M.; Gopalan, C. *Superlattices Microstruct.* **2003**, *34*, 459–465.
(62) Mitkova, M.; Kozicki, M. N.; Kim, H. C.; Alford, T. L. *Thin Solid Films* **2004**, *449*, 248–253.
(63) Black, J. R. *IEEE Trans. Electron Devices* **1969**, *16*, 338–347.
(64) Anariba, F.; Tiznado, H.; Diers, J. R.; Schmidt, I.; Muresan, A. Z.; Lindsey, J. S.; Zaera, F.; Bocian, D. F. *J. Phys. Chem. C* **2008**, *112*, 9474–9485.
(65) Wold, D. J.; Haag, R.; Rampi, M. A.; Frisbie, C. D. *J. Phys. Chem. B* **2002**, *106*, 2813–2816.
(66) Choi, S. H.; Kim, B.; Frisbie, C. D. *Science* **2008**, *320*, 1482–1486.
(67) Cho, M. Y.; Kang, H. S.; Kim, K.; Kim, S. J.; Joo, J.; Kim, K. H.; Cho, M. J.; Choi, D. H. *Colloids Surf., A* **2008**, *313−314*, 431–434.
(68) Facchetti, A.; Yoon, M.-H.; Marks, T. J. *Adv. Mater.* **2005**, *17*, 1705–1725.
(69) Kronemeijer, A. J.; Huisman, E. H.; Akkerman, H. B.; Goossens, A. M.; Katsouras, I.; van Hal, P. A.; Geuns, T. C. T.; van der Molen, S. J.; Blom, P. W. M.; de Leeuw, D. M. *Appl. Phys. Lett.* **2010**, *97*, 173302.
(70) Kim, B.; Beebe, J. M.; Jun, Y.; Zhu, X.-Y.; Frisbie, C. D. *J. Am. Chem. Soc.* **2006**, *128*, 4970–4971.
(71) Baheti, K.; Malen, J. A.; Doak, P.; Reddy, P.; Jang, S.-Y.; Tilley, T. D.; Majumdar, A.; Segalman, R. A. *Nano Lett.* **2008**, *8*, 715–719.
(72) Reddy, P.; Jang, S.-Y.; Segalman, R. A.; Majumdar, A. *Science* **2007**, *315*, 1568–1571.
(73) Venkataraman, L.; Park, Y. S.; Whalley, A. C.; Nuckolls, C.; Hybertsen, M. S.; Steigerwald, M. L. *Nano Lett.* **2007**, *7*, 502–506.
(74) Dell'Angela, M.; Kladnik, G.; Cossaro, A.; Verdini, A.; Kamenetska, M.; Tamblyn, I.; Quek, S. Y.; Neaton, J. B.; Cvetko, D.; Morgante, A.; Venkataraman, L. *Nano Lett.* **2010**, *10*, 2470–2474.
(75) Yaliraki, S. N.; Ratner, M. A. *J. Chem. Phys.* **1998**, *109*, 5036–5043.
(76) Xue, Y.; Datta, S.; Ratner, M. A. *J. Chem. Phys.* **2001**, *115*, 4292–4299.
(77) Stadler, R.; Jacobsen, K. W. *Phys. Rev. B* **2006**, *74*, 161405(R).
(78) Koch, N.; Kahn, A.; Ghijsen, J.; Pireaux, J.-J.; Schwartz, J.; Johnson, R. L.; Elschner, A. *Appl. Phys. Lett.* **2003**, *82*, 70–72.
(79) de Boer, B.; Hadipour, A.; Mandoc, M. M.; van Woudenbergh, T.; Blom, P. W. M. *Adv. Mater.* **2005**, *17*, 621–625.
(80) Akkerman, H. B.; Naber, R. C. G.; Jongbloed, B.; van Hal, P. A.; Blom, P. W. M.; de Leeuw, D. M.; de Boer, B. *Proc. Natl. Acad. Sci. U.S.A.* **2007**, *104*, 11161–11166.
(81) Heimel, G.; Romaner, L.; Zojer, E.; Bredas, J.-L. *Nano Lett.* **2007**, *7*, 932–940.
(82) Chun, W.-J.; Ishikawa, A.; Fujisawa, H.; Takata, T.; Kondo, J. N.; Hara, M.; Kawai, M.; Matsumoto, Y.; Domen, K. *J. Phys. Chem. B* **2003**, *107*, 1798–1803.
(83) George, C. B.; Ratner, M. A.; Lambert, J. B. *J. Phys. Chem. A* **2009**, *113*, 3876–3880.
(84) Heurich, J.; Cuevas, J. C.; Wenzel, W.; Schon, G. *Phys. Rev. Lett.* **2002**, *88*, 256803.
(85) Evers, F.; Weigend, F.; Koentopp, M. *Phys. Rev. B* **2004**, *69*, 235411.
(86) Ning, J.; Li, R.; Shen, X.; Qian, Z.; Hou, S.; Rocha, A. R.; Sanvito, S. *Nanotechnology* **2007**, *18*, 345203.
(87) Min, S. K.; Kim, W. Y.; Cho, Y.; Kim, K. S. *Nat. Nanotechnol.* **2011**, *6*, 162–165.
(88) Kim, W. Y.; Kwon, S. K.; Kim, K. S. *Phys. Rev. B* **2007**, *76*, 033415.
(89) Paulsson, M.; Frederiksen, T.; Brandbyge, M. *Nano Lett.* **2006**, *6*, 258–262.
(90) Ke, S.-H.; Baranger, H. U.; Yang, W. *J. Am. Chem. Soc.* **2004**, *126*, 15897–15904.
(91) Ke, S.-H.; Baranger, H. U.; Yang, W. *Phys. Rev. B* **2004**, *70*, 085410.
(92) Seminario, J. M.; De La Cruz, C. E.; Derosa, P. A. *J. Am. Chem. Soc.* **2001**, *123*, 5616–5617.
(93) Geng, W. T.; Nara, J.; Ohno, T. *Appl. Phys. Lett.* **2004**, *85*, 5992–5994.
(94) Cho, Y.; Kim, W. Y.; Kim, K. S. *J. Phys. Chem. A* **2009**, *113*, 4100–4104.
(95) McCreery, R. L. *Chem. Rev.* **2008**, *108*, 2646–2687.
(96) Arena, C.; Kleinsorge, B.; Robertson, J.; Milne, W. I.; Welland, M. E. *J. Appl. Phys.* **1999**, *85*, 1609–1615.
(97) Koivusaari, K. J.; Rantala, T. T.; Levoska, J.; Leppavuori, S. *Appl. Phys. Lett.* **2000**, *76*, 2794–2796.
(98) Mahmoud, A. M.; Bergren, A. J.; Pekas, N.; McCreery, R. L. *Adv. Funct. Mater.* **2011**, *21*, 2273–2281.
(99) Liu, Z.; Yasseri, A. A.; Lindsey, J. S.; Bocian, D. F. *Science* **2003**, *302*, 1543–1545.